Chapter 13
Comparative Analysis of Saturated Hydraulic Conductivity (K_{sat}) Derived from Image Analysis of Soil Thin Sections, Pedotransfer Functions, and Field-Measured Methods

Zamir Libohova, Philip Schoeneberger, Phillip R. Owens, Skye Wills, Doug Wysocki, Candiss Williams and Cathy Seybold

Abstract Saturated hydraulic conductivity (K_{sat}) is an important soil parameter that governs water movement through horizons, pedons, and soil landscapes. K_{sat} is infamous for its spatial and temporal variability, which contributes to the difficulty and considerable expense in measuring or otherwise quantifying it. Consequently, predictive methods such as pedotransfer functions (PTFs) that use physical soil properties, such as texture and bulk density, have been developed to derive K_{sat} values. Soil texture and structure are key factors influencing K_{sat} because of their direct relationship to pore size distribution. Quantitatively defining the combined effects of texture and structure on pore size distribution in a PTF is a difficult task. The objectives of this research were to: (i) estimate K_{sat} based on pore characteristics derived from soil thin sections via image analysis; and (ii) compare the resultant values with field-measured K_{sat} and with K_{sat} estimated by a PTF using soil texture and bulk density parameters. We digitally scanned 39 thin sections from 11 pedons of soils derived from loess over till and/or over weathered sandstone. Soil voids were classified based on their size and shape. K_{sat} was measured in the field using a Compact Constant-head Permeameter (Amoozemeter) and estimated using a Rosetta PTF. Simple and multiple linear regression (MLR) analyses were used to relate pore indexes and soil physical properties with measured and estimated K_{sat}. The mean measured K_{sat} was 0.74 cm h^{-1}, whereas the PTF-estimated K_{sat} from Rosetta and MLR were 0.36 cm h^{-1} and 0.49 cm h^{-1}, respectively. The addition of pore characteristics into the model improved K_{sat} predictions compared

Z. Libohova (✉) · P. Schoeneberger · S. Wills · D. Wysocki · C. Williams · C. Seybold
USDA-NRCS, Lincoln, NE, USA
e-mail: zamir.libohova@lin.usda.gov

P.R. Owens
Purdue University—Agronomy Department, West Lafayette, IN, USA

A.E. Hartemink and B. Minasny (eds.), *Digital Soil Morphometrics*,
Progress in Soil Science, DOI 10.1007/978-3-319-28295-4_13

to predictions using Rosetta alone. The estimated K_{sat} based on the model with added pore characteristics was better correlated with field-measured K_{sat} ($r = 0.82$) than that based on Rosetta ($r = 0.62$). The addition of pore characteristics can improve K_{sat} predictions. However, thin section void analysis from additional parent materials is needed.

Keywords Saturated hydraulic conductivity (K_{sat}) · Thin sections · Image analysis · Pedotransfer functions · Soil porosity

13.1 Introduction

The success of hydrology modeling predictions depends on the accurate representation of the spatial and temporal variability of major external drivers such as weather, land use, land management, geomorphic surface, and soil hydrological properties (Pachepsky et al. 2008). Saturated soil hydraulic conductivity (K_{sat}) is one of the most important soil parameters in hydrological modeling because it characterizes water movement through soils with direct and substantive impact on streamflow timing and volume (Guber et al. 2006). Unfortunately, K_{sat} is also one of the most difficult properties to accurately evaluate due to its variability over short-range distances (Oosterbaan and Nijland 1994) and over time. The presence of structural and/or root macropores has been identified as one of the major contributors to K_{sat} variability (White 1985; Perret et al. 1999, 2003; Watson and Luxmoore 1986). The terms "preferential flow" and "bypass flow" have been applied by many researchers to acknowledge the presence and the mechanisms of soil water movement through macropores (White 1985).

Although by definition K_{sat} is evaluated under saturated soil moisture conditions, the presence of macropores combined with the effects of "boundary conditions" between wet and dry soil matrices contributes to the variability in K_{sat} measurements and results in overestimations of K_{sat} (Bouma et al. 1989). Many field (in situ) and laboratory methods have been developed to overcome such limitations (Reynolds and Elrick 1985). Some of the field measurement methods include lysimeters (Barkle et al. 2010) and various constant or falling head permeameters (Amoozegar and Warrick 1986; Amoozegar 1989). Whether K_{sat} is measured in situ or in laboratory conditions, the methods have limitations related to the determination of an appropriate representative soil volume. A representative soil volume is needed to reduce the measurement variability due to preferential flow and wet/dry boundary conditions (Bouma et al. 1989; Mohanty and Mousli 2000). Techniques such as X-ray computed tomography (CT) have been developed to better evaluate the effects of macropores on K_{sat} by characterizing their size and distribution over a larger volume of soil and in a nondestructive manner (Anderson et al. 1990; Peyton et al. 1992, 1994). However, few studies exist on X-ray computed tomography (CT) methodology that link their results with other soil physical properties for

predictive K_{sat} (Peyton et al. 1994) and likewise other field methods are not very practical for routine measurements.

Most K_{sat} field methods and techniques are expensive and time-consuming and require many K_{sat} measurements over large areas and extended time periods to capture spatial and temporal variability. Bouma et al. (1989) discuss some of the morphological techniques for estimating the appropriate soil volume for representative measurements of K_{sat} in the field. They also recognized the challenges for upscaling such soil hydrological parameters for modeling (Bouma 2006). Different approaches to upscaling have been developed by researchers, but mostly rely on pedotransfer functions (PTFs) (Guber et al. 2006). McKenzie and Jacquier (1997) used successfully field soil morphological characteristics such as field texture, grade of structure, areal porosity, bulk density, dispersion index, and horizon type for K_{sat} predictions. Both visual and quantitative estimates of areal porosity provided satisfactory results, with the quantitative method performing slightly better (McKenzie and Jacquier 1997). The USDA-NRCS Kellogg Soil Survey Laboratory (KSSL) has approximately 8000 soil thin sections that offer a unique opportunity to quantify the role of porosity in improving K_{sat} predictions. Thin sections represent a small soil area and like in situ field K_{sat} measurements are scale limited. However, the incorporation of pore characteristics in modeling could potentially improve K_{sat} predictions. This chapter aimed to: (i) assess the use of soil thin sections to characterize the K_{sat} at the soil horizon level; and (ii) compare K_{sat} derived from thin sections with measured values and with values derived from a published PTF.

13.2 Materials and Methods

13.2.1 Study Sites and Soils

The two study sites selected for this research are in Wabash and Dubois Counties, Indiana. Soils in Wabash County are in the Northern Moraine and Central Till Plain Physiographic Region which is characterized by low-relief landscapes (Franzmaier et al. 2004). Soils in Dubois County are in the Southern Hills and Lowland Physiographic Region (Franzmaier et al. 2004), which is characterized by high-relief, bedrock-controlled hills (Franzmaier et al. 2004) (Fig. 13.1). Soils in study area formed predominantly in loess over till (Wabash County) or in loess over weathered materials from the underlying sandstone, siltstone, or shale (Dubois County) (Wingard et al. 1980). The texture class for the study soils is silt loam, silty clay loam, silty clay, or clay (Table 13.1).

The dominant soil series include Pewamo, Glynwood, and Blount in Wabash County and Wellston and Gilpin in Dubois County. Soil characterization analyses were conducted at the Kellogg Soil Survey Laboratory (KSSL) of USDA-NRCS, Lincoln, Nebraska.

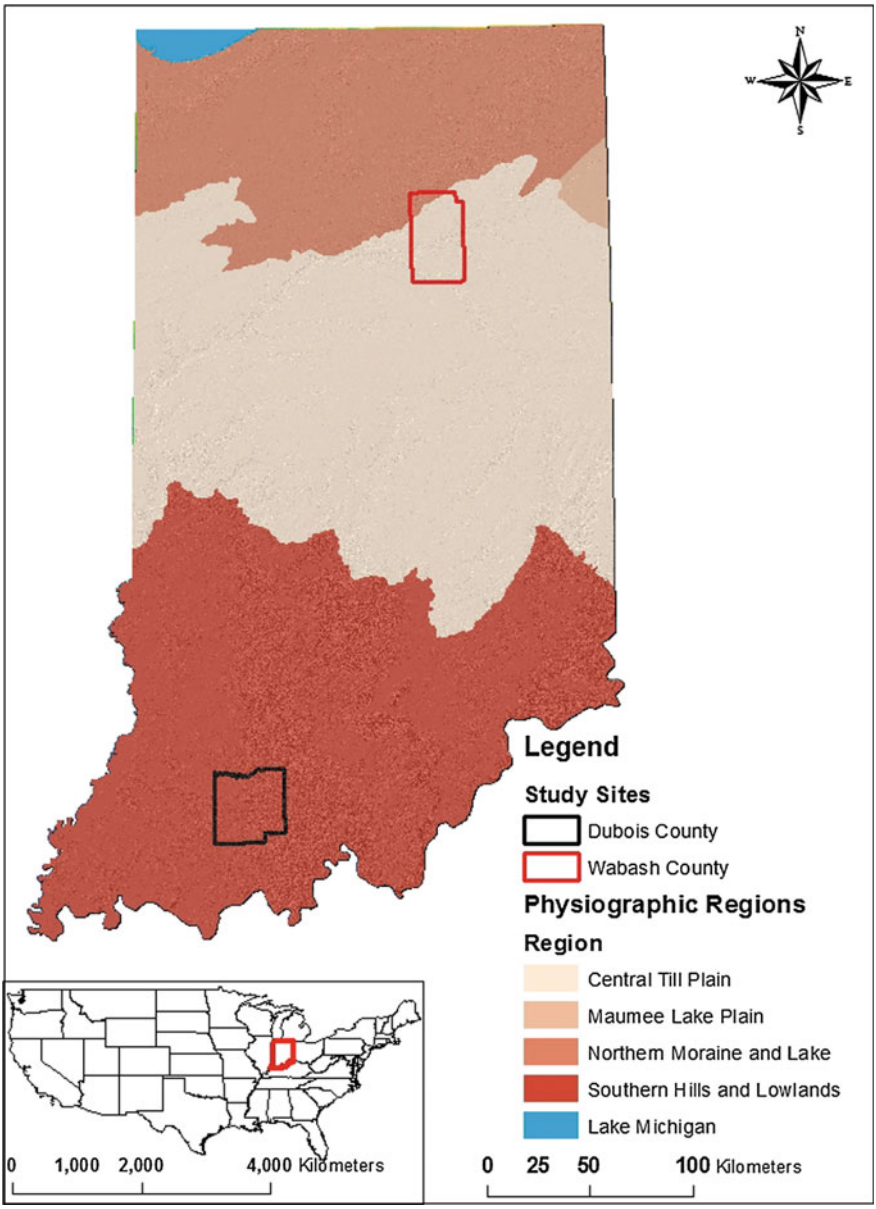

Fig. 13.1 Study site locations and physiographic regions of Indiana

Table 13.1 Measured physical characteristics of soils used for thin sections

County	Soil series	Texture class	Soil horizon	Particle size (<2 mm)			Bulk density		Water content	
				Clay (%)	Silt (%)	Sand (%)	33 kPa (g cm^{-3})	Oven Dry (g cm^{-3})	33 kPa (%wt)	1500 kPa (%wt)
Dubois	Wellston	SIL	Ap	20.3	76.9	2.8	1.46	1.52	24	8.7
	Wellston	SIL	Bt1	25.7	72.6	1.7	1.42	1.52	25.2	10.8
	Wellston	SIL	Btx	23.4	67.1	9.5	1.55	1.63	20.8	10.7
	Wellston	SIL	BA	25.5	72.8	1.7	1.45	1.58	24.8	11.2
	Wellston	SIL	Bt1	27.6	71.1	1.3	1.32	1.42	27.5	12.8
	Wellston	C	2Bt4	71.9	26.1	2	1.46	1.82	28.3	24
	Gilpin	SIL	Ap	23.9	68.5	7.6	1.49	1.61	23.1	12.7
	Gilpin	SICL	Bt1	28.2	64.2	7.6	1.48	1.58	23.7	13.3
	Gilpin	C	2Bt3	50.5	15.8	33.7	1.6	1.8	21.9	18.2
	Gilpin	SIL	Ap	24.6	56.9	18.5	1.38	1.49	26.1	11
	Gilpin	CL	Bt1	33	43.8	23.2	1.45	1.57	23.5	13.5
	Gilpin	CL	Bt3	34.2	44.6	21.2	1.59	1.78	21.4	13.3
	Gilpin	SIL	Ap	21	68.3	10.7	1.41	1.53	27.8	12.5
	Gilpin	SIL	2Bt1	25.9	58.8	15.3	1.53	1.67	21.6	9.6
	Gilpin	SIL	Ap	21.7	75.7	2.6	1.28	1.4	27.8	10.6
	Gilpin	SICL	Bt1	28	70.1	1.9	1.33	1.51	27.9	11.9
	Gilpin	SIL	2Btx	22.5	56.3	21.2	1.6	1.81	20.3	7.9
	Gilpin	C	3Bt1	38.7	34.1	27.2	1.53	1.85	24.6	15.1
	Gilpin	SIL	Ap	22.3	75	2.7	1.43	1.55	26.3	10.1
	Gilpin	SIL	Bt1	25	72.8	2.2	1.4	1.49	25.6	10.5
	Gilpin	SIL	Btx1	20.7	60.2	19.1	1.49	1.58	21.3	8.3
	Gilpin	SIL	Ap	20.9	75	4.1	1.48	1.61	24.3	10.3
	Gilpin	SIL	Bt1	22.6	67.7	9.7	1.49	1.56	21.9	8.8
	Gilpin	SICL	2Btx1	27.9	58.7	13.4	1.52	1.66	22.6	10.1

(continued)

Table 13.1 (continued)

County	Soil series	Texture class	Soil horizon	Particle size (<2 mm)			Bulk density		Water content	
				Clay (%)	Silt (%)	Sand (%)	33 kPa (g cm^{-3})	Oven Dry (g cm^{-3})	33 kPa (%wt)	1500 kPa (%wt)
Wabash	Pewamo	SICL	Ap1	29.4	52.6	18	1.53	1.64	20.2	15.3
	Pewamo	SIC	Btg2	45	43.9	11.1	1.49	1.72	24.4	18.2
	Pewamo	SIC	BCdtk	54.2	38.1	7.7	1.59	1.82	23.2	20.1
	Pewamo	C	Cdk2	54.1	38.9	7	1.64	1.88	23.2	20.4
	Glynwood	SICL	Ap1	28	53.1	18.9	1.69	1.83	18.9	12.7
	Glynwood	SICL	Bt2	34.6	37.7	27.7	1.51	1.73	22.1	16.9
	Glynwood	SIC	BCdtk	34.4	42.7	22.9	1.51	1.73	23.9	14.2
	Glynwood	SIC	Cdk2	35.3	42.9	21.8	1.8	1.94	17.4	14.4
	Glynwood	SICL	Ap	26.4	54.4	19.2	1.57	1.7	19.3	12.4
	Glynwood	CL	Bt2	49	38.7	12.3	1.46	1.73	24.3	20.3
	Glynwood	CL	Cdtk	40.9	42.3	16.8	1.63	1.88	20.4	16
	Glynwood	CL	Cdk2	25.9	51.1	23	1.8	1.9	15.4	11.2
	Blount-Del Rey	SICL	Ap	35.4	46.9	17.7	1.71	1.89	18.7	14.8
	Blount-Del Rey	C	Bt2	51.8	38.6	9.6	1.54	1.88	24.7	18.7
	Blount-Del Rey	SIC	Cdk1	52.1	40.3	7.6	1.64	1.88	22.5	18.3
	Blount-Del Rey	SIC	Cdk3	49.7	41.5	8.8	1.69	1.91	21.4	18.9

13.2.2 Thin Section Image Processing and Analysis

We selected 39 horizons with prepared thin sections from 11 pedons. The horizons were grouped as Ap (surface), Bt (subsurface), and C horizons (deepest). The thin section dimensions were 2.0 × 3.5 cm, but we avoided the section edges during scanning to minimize sample preparation artifacts. We analyzed pores via a three-step process:

Step 1 Thin sections were scanned with an HP Officejet 6310 and edited with HP Photosmart Software before image analysis. The scanned image resolution was set at 7200 dpi and saved in "bmp" format, which is compatible with ENVI (Environment for Visualizing Images, Version 3.2, Research Systems Inc., Boulder, Colorado) image analysis software. We performed an image enhancement before exporting the image to ENVI (Fig. 13.2a). The enhancement process included brightness and contrast adjustments to highlight pores by increasing contrast between the soil matrix and the voids. This enhancement allowed a simple and efficient image classification

Step 2 We imported the enhanced image into ENVI as RGB and transformed it to hue, saturation, and value (HSV) formats (Fig. 13.2b). The density slicing

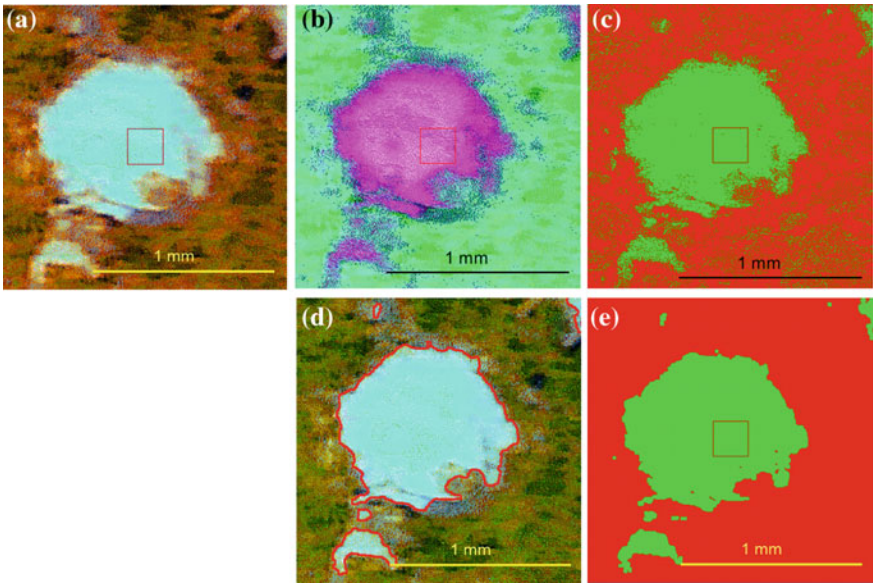

Fig. 13.2 A portion of a thin section illustrating the processing steps: **a** enhancement; **b** RGB to HSV density slicing; **c** unsupervised classification; **d** filtering; and **e**) vectorization used to derive pore characteristics

function was used to define the wavelength ranges for major colors (red, green, blue, yellow, cyan, magenta maroon, and sea green) of HSV-converted thin sections. Color ranges for the voids were identified and the image was segmented, which yielded an image of two contrasting colors that represented either the soil matrix or voids

Step 3 We used an unsupervised classification to evaluate the image and then a "sieve" function to remove isolated pixels (Fig. 13.2c). The binary image (matrix and voids) was further processed using majority filter (kernel size = 5), clumped (kernel size = 5), and majority filter (kernel size = 11) (Fig. 13.2d). The resulting binary image was converted to a vector file using ENVI and exported as a shape file (Fig. 13.2e). The polygon shape file was further processed in ArcMap (ESRI 2009) for soil pore classification

13.2.3 Soil Pore Classification

After image processing, small isolated polygons (outliers) were either combined with adjacent polygons or eliminated. There is no agreement in pore size classifications used for distinguishing between micropores and macropores (Bouma et al. 1979). Moreover, the naming convention is inconsistent: Some authors use a two-term "micro-" and "macro"-pores distinction (Jongerius 1957; Bouma et al. 1977), whereas others use a multi-term description such as "very fine," "fine," "coarse," etc. (Russell 1973; Soil Survey Division Staff 1993). The equivalent cylindrical diameter (ECD) ranges associated with pore size categories are also inconsistent across studies. In all of the studies we reviewed, pore size is based on ECD rather than mean equivalent square (MEC), which is the shape of pixels and the resulting polygons produced by thin section image analysis. To remove the remaining small square polygons, we calculated the area of a single pixel based on the 7200 dpi resolution and dimensions. The area of a pixel was calculated to be 12.0 μm^2, which is approximately a 3.44 × 3.44 μm square. To use ECD for distinguishing micropores and macropores, the square pixel dimension was assumed to also represent a circular pore diameter. The ECD was calculated based on the "area" column in the polygon attribute shape file and the pixel dimensions derived from the image resolution. A threshold value of 200 pixels was used to separate micropores from macropores. Polygons with an area greater than 200 pixels were further classified into three major shapes, as per Bouma et al. (1977), using void area (A)/void perimeter (P^2) ratio with A/P2 > 0.04 classified as "rounded"; A/P2 < 0.04 and >0.015 as "intermediate"; and A/P2 < 0.015 as "elongated" voids.

13.2.4 Soil-Saturated Hydraulic Conductivity (K_{sat})

Field-Measured K_{sat}

The K_{sat} values were determined from in situ measurements using a Compact Constant-Head Permeameter (Amoozometer) (Amoozegar 1989; Amoozegar and Warrick 1986). The in situ K_{sat} was determined for major soil horizons from which the thin sections were extracted, each in five replicates. The major horizons were (i) surface or near surface horizons (Ap, E, AB, BE); (ii) subsurface horizons (Bt1, Bt3); and (iii) deeper restrictive horizons (Btx, 3Bt, Cr). The replicates were spaced approximately 1 m apart and aligned along topographic contours.

Pedotransfer Function (PTF) Estimated K_{sat}

We used a pedotransfer function software Rosetta V1.0 to estimate K_{sat} based on soil texture (sand, silt, clay), bulk density, and water content at 33 and 1500 kPa water tension (Schaap et al. 1998). The soil input parameters for Rosetta were measured values from the KSSL characterization data. In addition to Rosetta, we also estimated K_{sat} using a step-wise multiple linear regression (MLR) model that included porosity characteristics (total porosity and pore shape) as well as soil texture (sand, silt, clay), bulk density, and water content at 33 and 1500 kPa water tension.

13.2.5 Statistical Analysis

We used Pearson's correlation coefficient to assess the relationship between measured K_{sat} and estimated K_{sat} from Rosetta and step-wise multiple linear regression (MLR) analysis. We also employed forward step-wise regression analysis to determine the best K_{sat} predictors. We evaluated R^2, RMSE (root-mean-square error), and Akaike Information Criterion (AIC) (Akaike 1974, 1976) criteria to select the best K_{sat} predictive model. LSMeans Tukey's HSD test was used to compare mean K_{sat} between different soil horizons. The mean comparison test was done on the log-transformed data due to non-normal distribution. The null hypotheses were rejected at a significance level of 0.05. The statistical analysis was conducted in JMP (SAS Institute Inc. 2003).

13.3 Results and Discussions

13.3.1 Pore Size Distribution from Thin Sections

We grouped soil horizons into three major layers (L1, L2, L3) based on morphological, physical, and chemical characteristics (Table 13.2). There were no differences in mean pore radius between surface (L1), intermediate (L2), and deepest horizons (L3). Similar results are reported by Bouma et al. (1977) who found no specific, significant trends with depth for the three macropore types. Total porosity for the surface layer was slightly higher than that for the intermediate layer; however, both layers (L1, L2) had lower total porosity than the deepest layer (L3).

The proportions of different pore shapes relative to total porosity showed mixed trends with soil depth, especially for the deepest layer. Differences were slight for the upper and intermediate layers and greatest for the deepest layer. For example, proportions of elongated pores in the deepest layer (L3) were higher than those of the upper layers (L1, L2), whereas proportions of rounded pores and, especially, intermediate pores in the deepest layer (L3) were less than half of those of the upper layers (L1, L2). Bouma et al. (1977) observed similar tendencies of increasing proportions of elongated pores with depth and determined that the water flow along structural channels was the main mechanism for water movement.

13.3.2 Estimated K_{sat} from Step-Wise Multiple Regression Analysis

In addition to the Rosetta parameters used for predicting K_{sat} (sand, silt, clay, bulk density, and water content at 33 kPa and 1500 kPa), we added the following parameters to the model: pore characteristics derived from thin section image analysis (total porosity, pore radius, elongated/total porosity ratio, rounded/total porosity ratio, and intermediate/total porosity) (Table 13.3).

Table 13.2 Pore characteristics from image analysis of thin sections

Grouped soil horizons	Genetic soil horizons	Pore radius (μm)	Total porosity (%)	Elongated/total porosity	Rounded/total porosity	Intermediate/total porosity
L1	Ap, Ap1, BA	5.5 (0.37)	12.4 (3.02)	68.2 (5.00)	3.8 (0.97)	28.1 (4.29)
L2	Bt1, Bt2, 2Bt1, 2Btx, 2Btx1, BCdtk, Cdk2	5.4 (0.30)	10.7 (2.54)	67.9 (4.20)	3.9 (0.81)	28.0 (3.61)
L3	Bt3, Btg, Bt3, 2Bt4, 3Bt1, BCdtk, Cdtk, Cdtk (1, 2, 3)	5.9 (0.40)	18.8 (3.31)	82.4 (4.48)	3.1 (1.06)	14.5 (4.70)

Numbers in parentheses are standard error values

Table 13.3 Parameter estimates and significance from step-wise multiple regression (MLR) analysis and Rosetta PTF for predicting saturated soil hydraulic conductivity (K_{sat})

Predictive parameter	Step-wise MLR					Rosetta		
	Full	Texture	Texture Bd	Texture Bd/WC	Porosity	Texture	Texture Bd	Texture Bd/WC
Pore_radius (μm)	x				x			
Total porosity (%)	x*				x			
Elongated/total (%)	x				x			
Rounded/total (%)	x*				x			
Intermediate/total (%)	x*				x			
Clay (%)	x	x	x	x		x	x	x
Silt (%)	x	x	x	x		x	x	x
Sand (%)	x*	x	x	x		x	x	x
Bd at 33 kPa (g cm^{-3})	x*		x	x			x	x
Bd oven dry (g cm^{-3})	x		x	x			x	x
WC at 10 kPa (%wt)	x*			x				x
WC at 33 kPa (%wt)	x			x				x
WC at 1500 at kPa (%wt)	x*			x				x
R^2	0.82	0.04	0.10	0.12	0.10	0.01	0.09	0.05
RMSE	1.64	2.36	2.30	2.28	2.43	2.41	2.32	2.36

Texture refers to clay, silt, and sand fractions; Bd is the soil bulk density; WC is the soil water content
*Parameters significant at p value = 0.05

This model yielded the highest R^2 (0.82) (adjusted R^2 = 0.70). The resultant prediction equation is given as:

$$K_{sat} = 238 + -0.12 * TP + 0.82 * R/T + -0.28 * I/T + -2.85 * \text{Sand} + -94.88 * \text{Bd33} + -3.71 * \text{WC10} + 0.35 * \text{WC1500} + 12.12 * \text{WC33}$$

where TP is the total porosity; R/T is the ratio of rounded pores over total pores; I/T is the ratio of intermediate pores over total pores; Sand is the total sand (%); Bd33 is the bulk density (g cm^{-3}) at 33 kPa water tension; WC10 is the water content (wt%) at 10 kPa tension; WC1500 is the water content (wt%) at 1500 kPa tension; and WC33 is the water content (wt%) at 33 kPa tension. Interestingly, both step-wise multiple linear regression (MLR) and Rosetta showed similar performance when

only soil texture, bulk density, and water content were used for K_{sat} predictions (Table 13.3). Also, when the statistical parameters of the step-wise MLR model included only pore characteristics, the resulting R^2 was 0.10 and RMSE was 2.43. It is possible that the use of a larger number of parameters in the step-wise MLR model resulted in better predictions compared to Rosetta PTF. Unfortunately, for this study we did not have a way to compare both models using all parameters including porosity, as Rosetta PTF was developed based on soil texture, bulk density, and water content only. Also, the comparisons between step-wise MLR and Rosetta models were based on a small sample size (n = 39). We recognize the unfairness with regard to the use of porosity for the step-wise MLR and a small sample size for both models. These are especially critical for Rosetta that was developed on much larger sample size and did not incorporate as many parameters as step-wise MLR. However, the results indicate that a combination of both physical soil properties and pore characteristics is needed to improve K_{sat} predictions. More data are needed on thin sections and other described soil morphological characteristics that relate to structure and pore size as shown by McKenzie and Jacquier (1997).

13.3.3 Measured Versus Estimated K_{sat} from Rosetta and Step-Wise Multiple Linear Regression Analysis

There were significant differences in mean K_{sat} values between grouped soil horizons (L1, L2, L3), especially for the deepest layer (L3). With the exception of the Rosetta PTF model, the K_{sat} values decreased exponentially with depth (Table 13.4). The decrease in K_{sat} by an order of magnitude with soil depth, especially between the surface and the subsurface layers, has been observed by others (Lin 2006). The measured K_{sat} values were more variable compared to those from the Rosetta PTF and Step-Wise MLR models, as shown by standard error values in parentheses in Table 13.4. This is to be expected due to the fact that measured K_{sat} values derived at field point scale are more prone to local variability in actual measured soil volume surrounding the instrument, which depends upon soil structure and, more specifically, pore size and distribution (Bouma et al. 1989).

Rosetta PTF and, to a lesser degree, the step-wise MLR model over-fit the data, resulting in less variability in predicted K_{sat} values compared to measured values. The role that soil structure, especially pore size, shape, and distribution, plays in predicting K_{sat} is well documented (Bouma et al. 1989; White 1985; Perret et al. 1999, 2003). However, one of the major limitations of Rosetta PTF is the lack of soil structure input parameters. The Rosetta PTF model uses soil texture, bulk density, and soil water retention characteristics to predict K_{sat} (Schaap 1999; Schaap et al. 1998), none of which is a direct representation of the soil structure. The addition of pore characteristics to the model may improve the prediction of K_{sat} values (Fig. 13.3).

Table 13.4 Mean comparisons between measured K_{sat} and those derived from Rosetzta PTF, and step-wise multiple linear regression model

Grouped soil horizons	Genetic soil horizons	Measured		Rosetta		Step-Wise MLR	
		Mean** (cm h^{-1})	Sig* (cm h^{-1})	Mean** (cm h^{-1})	Sig* (cm h^{-1})	Mean** (cm h^{-1})	Sig* (cm h^{-1})
L1	Ap, Ap1, BA	2.10 (0.98)	a	0.51 (0.08)	a	1.04 (0.23)	a
L2	Bt1, Bt2, 2Bt1, 2Btx, 2Btx1, BCdtk, Cdk2	0.22 (0.81)	a	0.39 (0.06)	a	0.27 (0.09)	b
L3	Bt3, Btg, 2Bt3, 2Bt4, 3Bt1, BCdtk, Cdtk, Cdtk (1, 2, 3)	0.04 (1.40)	b	0.15 (0.03)	b	0.05 (0.02)	c
		0.74 (0.38)	**a**	**0.36 (0.04)**	**a**	**0.49 (0.12)**	**a**

The reported values are in their "native" format but the mean comparisons are based on log-transformed values. Numbers in parentheses are standard error values

*Significant at p value = 0.05

**Mean values within the same method followed by same letters are not significantly different. Mean values between methods (bold) followed by same letters are not significantly different

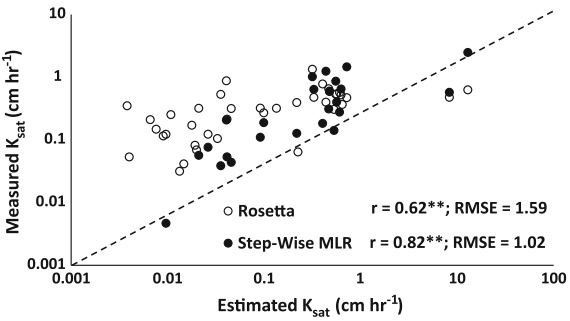

Fig. 13.3 Estimated versus measured K_{sat} values based on Rosetta and step-wise multiple regression model (MLR)

The results are promising. However, they are based on a small data set and broader evaluation is needed. The K_{sat} method we developed from thin sections has limitations like any other proxy method used to measure or estimate K_{sat}. Thin sections represent a small soil area and do not show three-dimensional pore continuity patterns, particularly for macropores, which control K_{sat} at horizon and pedon scales (Bouma et al. 1977). Whether measured K_{sat} is determined in situ or in a laboratory setting, identifying the appropriate representative soil volume, which is needed to reduce the variability due to preferential macropore flow, is challenging

(Bouma et al. 1989; Mohanty and Mousli 2000). Techniques such as X-ray computed tomography (CT) have been developed to better evaluate the effects of macropores on K_{sat} by characterizing their size, distribution, and, especially, connectivity over a large volume of soil in a nondestructive manner (Anderson et al. 1990; Peyton et al. 1992, 1994). However, X-ray computed tomography (CT) despite advantages is expensive. In addition, there is no extensive data available to our knowledge with both X-ray computed tomography (CT) analysis and soil physical properties for developing predictive K_{sat} models.

13.4 Conclusions

Soil-saturated hydraulic conductivity (K_{sat}) is one of the most important properties used to describe soil water movement. However, K_{sat} is highly variable and measuring it in the field is expensive. Pedotransfer functions (PTFs) such as Rosetta use soil physical properties (texture and bulk density) to predict K_{sat}. Soil morphological properties, especially porosity, can be added to PTF models to improve K_{sat} prediction. We used soil thin sections and image analysis to help quantify pore size and shape from soils for which measured K_{sat} values were available.

Pore characteristics alone explained 10 % of the predicted K_{sat} variability. Including them in PTF models with the other soil physical properties improved the K_{sat} predictions for loess-derived soils in our study area. The pore numerical quantification from thin sections is limited because of the lack of an appropriate representative soil volume, which is needed to overcome the high variability of K_{sat} due to preferential flow as related to the presence of soil macropores.

The results from this study show the potential of pore characteristics to improve K_{sat} prediction, but additional studies are needed on soils derived from other parent materials and with texture ranges wider than loess. The USDA-NRCS Kellogg Soil Survey Laboratory (KSSL) has over 8000 soil thin sections that could be used to assess the potential of using pore characteristics to improve K_{sat} predictions.

References

Akaike H (1974) A new look at the statistical model identification. IEEE Trans Autom Control 19:716–723

Akaike H (1976) An information criterion (AIC). Math Sci 14:5–9

Amoozegar A (1989) A compact constant-head permeameter for measuring saturated hydraulic conductivity of the vadoze zone. Soil Sci Soc Am J 53:1356–1361

Amoozegar A, Warrick AW (1986) Hydraulic conductivity of saturated soils: field methods. In: A. Klute (ed) Methods of soil analysis. Part I. Physical and mineralogical methods. 2nd edn. Agronomy Series, vol. 9, American Society Agronomica, pp. 735–770

Anderson SH, Peyton RL, Gantzer CJ (1990) Evaluation of constructed and natural soil macropores using X-ray computed tomography. Geoderma 46:13–29

Barkle GF, Wöhling Th, Stenger R, Mertens J, Moorhead B, Wall A, Clague J (2010) Automated equilibrium tension lysimeters for measuring water fluxes through a layered, volcanic vadose profile in New Zealand. Vadose Zone J 10:747–759. doi:10.2136/vzj2010.0091

Bouma J (2006) Hydropedology as a powerful tool for environmental policy research. Geoderma 131:275–286

Bouma J, Jongerius A, Boersma O, Jager A, Schoonderbeek D (1977) The function of different types of macropores during saturated flow through four swelling soil horizons. Soil Sci Soc Am J 41:945–950

Bouma J, Jongerius A, Schoonderbeek D (1979) Calculation of hydraulic conductivity using micromorphometric data. Soil Sci Soc Am J 43:261–264

Bouma J, Jongmans AG, Stein A, Peek G (1989) Characterizing spatially variable hydraulic properties of a boulder clay deposit in The Netherlands. Geoderma 45:19–29

ESRI (2009) ArcGIS desktop: release 9. Environmental Systems Research Institute, Redlands, CA

Franzmaier DP, Steinhardt GC, Schulze DG (2004) Indiana soil and landscape evaluation manual, version 1.0. Purdue University, Agronomy Department

Guber AK, Pachepsky YA, van Genuchten MTh, Rawls WJ, Simunek J, Jacques D, Nicholson TJ, Cady RE (2006) Field-scale water flow simulations using ensembles of pedotransfer functions for soil water retention. Vadose Zone J 5:234–247

Jongerius A (1957) Morphologic investigations of soil structure. Bodemkundige Studies No. 2. Mededelingen van de Stickting voor Bodemkartering, Wageningen, The Netherlands

Lin H (2006) Temporal stability of soil moisture spatial pattern and subsurface preferential flow pathways in the Shale Hills catchment. Vadose Zone J 5(1):317–340

McKenzie N, Jacquier D (1997) Improving the field estimation of saturated hydraulic conductivity in soil survey. Aust J Soil Res 35(4):803–827

Mohanty BP, Mousli Z (2000) Saturated hydraulic conductivity and soil water retention properties across a soil-slope transition. Water Resour Res 43(11):3311–3324

Oosterbaan RJ, Nijland HJ (1994) Determining the saturated hydraulic conductivity, chapter 12. In: Ritzema HP (ed) Drainage principles and applications. International Institute for Land Reclamation and Improvement (ILRI), Pub. 16, 2nd revised edn. Wageningen, The Netherlands, ISBN 90 70754 3 39

Pachepsky YA, Gimenez D, Lilly A, Nemes A (2008) Promises of hydropedology. Perspect Agric Vet Sci Nutri Nat Resour 3:2–19

Perret JS, Prasher SO, Kantzas A, Langford C (1999) Three-dimensional quantification of macropore networks in undisturbed soil cores. Soil Sci Soc Am J 63:1530–1543

Perret JS, Prasher SO, Kacomov AR (2003) Mass fractal dimension of soil macropores using computed tomography: From the box-counting to the cube-counting algorithm. Europ J Soil Sci 54:569–579

Peyton RL, Haeffner BA, Anderson SH, Gantzer CJ (1992) Applying X-ray CT to measure macropore diameters in undisturbed soil cores. Geoderma 53:329–340

Peyton RL, Gantzer CJ, Anderson SH, Haeffner BA, Pfeifer P (1994) Fractal dimension to describe soil macropore structure using X-ray computed tomography. Water Resour Res 30 (3):691–700

Reynolds WD, Elrick DE (1985) In-situ measurement of field saturated hydraulic conductivity, sorptivity, and the a-parameter, using the Guelph permeameter. Soil Sci 140(4):292–302

Russell EW (1973) Soil conditions and plant growth, 10th edn. Longmans, London

SAS Institute Inc. (2003) JMP®, Version 11.0.0. Cary, NC

Schaap MG (1999) Rosetta (http://www.ussl.ars.usda.gov/MODELS/rosetta/rosetta.htm)

Schaap MG, Leij FJ, van Genuchten MTh (1998) Neural network analysis for hierarchical prediction of soil water retention and saturated hydraulic conductivity. Soil Sci Soc Am J 62:847–855

Soil Survey Division Staff (1993) Soil survey manual. Soil conservation service. U.S. Department of Agriculture Handbook 18

Watson KW, Luxmoore RJ (1986) Estimating macroporsity in a forest watershed by use of a tension infiltrometer. Soil Sci Soc Am J 50:578–582

White RE (1985) The influence of macropores on the transport of dissolved and suspended matter through soil. Adv Soil Sci 3:95–120

Wingard RC, Bernard JR, Coulter GW, Hudson GL (1980) Soil survey of Dubois County, Indiana. United States Department of Agriculture, National Cooperative Soil Survey. U.S. Government Printing Office 299-473/87, 117 p